IOP Publishing Journal of Micromechanics and Microengineering
J. Micromech. Microeng. **28** (2018) 014007 (11pp) https://doi.org/10.1088/1361-6439/aa9e25

Soft-rigid interaction mechanism towards a lobster-inspired hybrid actuator

Yaohui Chen[1], Fang Wan[2], Tong Wu[1] and Chaoyang Song[1]

[1] Mechanical Engineering, Monash University, Clayton, Victoria, Australia
[2] Independent Researcher, Wuhan, Hubei, People's Republic of China

E-mail: songcy@ieee.org

Received 1 September 2017, revised 15 November 2017
Accepted for publication 29 November 2017
Published 15 December 2017

Abstract

Soft pneumatic actuators (SPAs) are intrinsically light-weight, compliant and therefore ideal to directly interact with humans and be implemented into wearable robotic devices. However, they also pose new challenges in describing and sensing their continuous deformation. In this paper, we propose a hybrid actuator design with bio-inspirations from the lobsters, which can generate reconfigurable bending movements through the internal soft chamber interacting with the external rigid shells. This design with joint and link structures enables us to exactly track its bending configurations that previously posed a significant challenge to soft robots. Analytic models are developed to illustrate the soft-rigid interaction mechanism with experimental validation. A robotic glove using hybrid actuators to assist grasping is assembled to illustrate their potentials in safe human-robot interactions. Considering all the design merits, our work presents a practical approach to the design of next-generation robots capable of achieving both good accuracy and compliance.

Keywords: soft pneumatic actuators, hybrid actuators, soft-rigid interaction mechanism, lobster-inspired

(Some figures may appear in colour only in the online journal)

1. Introduction

The drive towards wearable robotic devices motivates the research in safe human-robot interaction, and these devices can find widespread potential applications targeted at biomedical rehabilitation or assistance of daily activities. Implementation of traditional articulated structures is with the ease of design, modeling, fabrication, and control [1]. However, it also presents challenges in the safety issue mainly due to the lack of viable actuation strategies to provide necessary compliance. Although some solutions have been proposed to compensate for the low mechanical compliance of these structures, including adopting adaptive control strategies and more advanced actuation mechanisms [2], they significantly increase the mechanical complexity and usually lead to a bulky design [3].

Recently, a more bio-inspired method has been suggested to develop robots using soft materials to achieve a high compliance. These soft robots can move like soft-body animals and utilize actuation methods that are intrinsically soft, flexible and compliant. Silicone-based soft pneumatic actuators (SPAs), which are the pioneering genre of soft robotics, have drawn a lot of attention due to their light weight, low fabrication costs, and desirable output in the range of force and motions [4, 5]. These actuators are usually composed of air corridors and chambers, and adopt fiber or other strain limiting materials to modify the bending configurations. They have been shown to be potentially very useful in human-assistive or wearable robotic devices that can replicate the motion of parts of the body [6], restore joint function [7–9] or assist daily activities [10, 11]. However, the continuous deformation of fully soft components is beyond the scope of the classic robotic theory, and new solutions for sensor integration and fine control are needed. While some stretchable sensors have been developed to measure the pressure or strain of soft systems [12, 13], it is still challenging to measure their exact deformation.

In more recent designs, hybrid robotic actuators have also been proposed with both rigid and soft components. Introducing rigid structures into soft robots can potentially lead to increased controllability and reliability, as these rigid

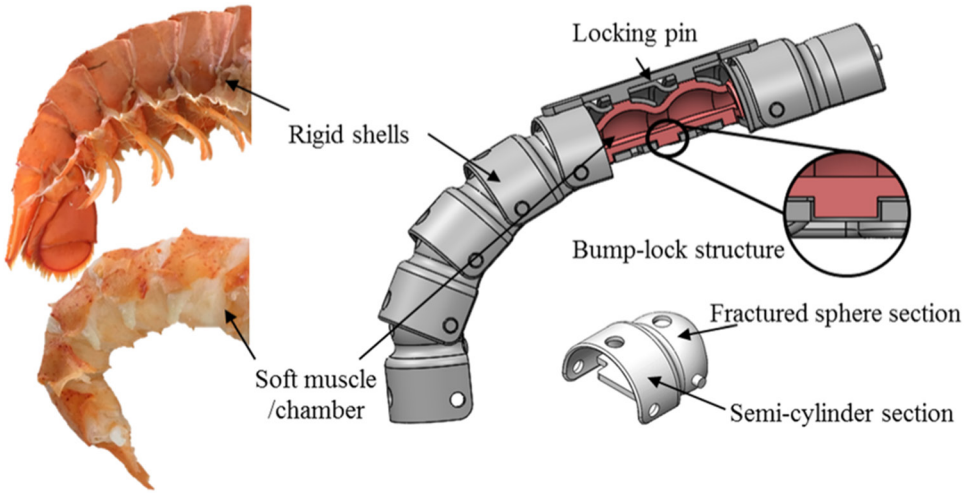

Figure 1. The lobster-inspired hybrid actuator design that consists of rigid shells and a soft chamber inside.

structures can constrain and predefine the deformation of soft robots. A similar approach has already been adopted in some origami-inspired designs [14, 15], where a inflatable soft component is used to actuate the origami structures even with on-board sensing [16]. Moreover, soft materials have also been assembled into multilayer rigid-flex laminates in millimeter scale to achieve both safe actuation and more effective force transmission [17]. Such a design strategy makes hybrid actuators promising to achieve a high compliance while maintaining the ease of analysis and control at the same time.

In our previous work, we have introduced a first proof of the hybrid actuator design inspired by the anatomical structure of lobster's abdomen, in which the soft chamber can be fully protected and the actuator has exactly defined joint and link structures at the same time. This is realized by integrating a soft chamber into articulated rigid shells, and the hybrid actuators can therefore generate compliant and controllable motion in a wider pressure range. Moreover, the actuator's motion can be described using the kinematic model, which is significantly different from purely soft systems. In one type of proposed hybrid actuators, we consider the inner soft chamber as a tubular chamber for the ease in design and fabrication. Analytic models have been developed to characterize this actuator's bending and force exerting capacity [18], and we developed a robotic glove based on it to facilitate a safe and comfortable rehabilitation process [19]. To minimize fatiguing of the soft material and improve the durability of the hybrid actuator, we then modify the soft chamber into a bellow-type chamber that creates motions by unfolding and folding the bellows [19]. In this way, the soft chamber undergoes smaller volume change and strains upon actuation as suggested by [20]. The hybrid actuator can also be actuated more rapidly as the rigid shells better constrain the radial expansion of the soft chamber.

In this paper, we further extend the work on the hybrid actuator with a bellow-type soft chamber. We present an easy fabrication method that requires the least equipment and time compared with that of typical SPAs, and develop analytic models to illustrate the soft-rigid interaction mechanism in our proposed hybrid actuator. We also conduct comprehensive experimental tests for both actuator characterization and model validation with fabricated hybrid actuators. Especially, we focus on the coupling of input pneumatic pressure, bending configurations and output tip force, and aim to demonstrate how the soft-rigid interaction mechanism could enable the hybrid actuator design. Finally, based on the results obtained from the characterization of the hybrid actuators, we assemble four hybrid actuators into a robotic glove that can assist grasping. The idea is that hybrid actuators can provide compliant actuation to ensure safety and comfortability, and based on the analytic models developed we can easily predict the grasping force. Such articulated structures can also be easily sensed in both bending configurations and force exertion, which will be conducted in the future work. In this paper, we are not focused on the design of a specific robotic system that can assist daily activities, but on how the proposed strategy can potentially enable such an design.

2. Methods

2.1. Lobster-inspired design

A challenging environment is presented for any organism in the littoral region of the ocean, for fundamental problems exist including crushing from sharp objects, turbulence caused by surge or tides, hunting from predators and chemical stimulus [21]. However, bottom-dwelling organisms, like lobsters, have navigated in these complex conditions with impunity since 140 million years ago [22], and have evolved robust systems for locomotion, self-protection, sensing and searching [23]. The abdomen of a lobster has a unique structure that consists of soft muscles enclosed by an array of rigid shells hinged in serial, as shown in figure 1. The rigid shells serve for protection against predators and stabilize the whole lobster body. These shells have a multi-layer structure composed of chitin-proteins, and the presence of biomineral particles such as amorphous calcium carbonate and calcite further harden these shells [24]. This distinct microstructure provides the lobster

an optimal performance in both flexibility and mechanical strength during an active bending motion [25]. One can usually consider the shell segment as a rigid component, as its stiffness can reach values of around 10 GPa in both normal and transverse direction [26].

On the other hand, the soft muscle inside the lobster abdomen also plays an important part in the lobster's underwater survival. Tendinous cells intervene between the soft tissue and the rigid shells for motion transmissions [27], which enable the lobster abdomen to function as an actuator that generates a powerful tail-flip motion [28]. It is an important survival technique for the lobsters when predators attack them. In this situation, the soft muscle can selectively drag or push the shells and accurately control the abdomen region to bend, thus propelling the lobsters with high velocity to swim away in the backward direction [28]. These soft muscles can also actuate the shells through hydrostatic effects so that the crustaceans can still locomote during molting, a period during which the new layers of the shells have generated but not yet hardened [29].

To mimic such an actuation behavior, we propose a hybrid robotic actuator consisting of rigid shells and a soft chamber enveloped inside. The fractured sphere section of the previous rigid shell can be fully folded into the semi-cylinder part of the next one, thus providing full protection to the deformed soft chamber under fluidic pressurization. The soft chamber is designed to maximumly fill the internal volume of the rigid shells hinged in series. Moreover, we introduce bump-lock structures to realize self-locking during actuation. Half of the bump-lock structures lie on the top of the fractured sphere part of the rigid shells to lock each bellow head, and the other half are positioned at each joint where there should be theoretically minimal sliding. Once pressurized, such hybrid structure will also produce a hydrostatic effect during the interaction between the soft chamber and the rigid shells, providing a rotary motion about each joint axis and an overall bending movement like the lobster abdomen [19].

An important aspect of the proposed lobster-inspired actuator design is the balanced functions of the rigid and soft components through mechanical interaction. The soft chamber produces both active drives as well as passive compliance under fluidic pressurization, and it can sustain higher pressure and produce enhanced output with the rigid protection. The rigid constraints also predefine the kinematics of the overall actuator and regulate the bending into a multi-link structure. This articulated structure can better perform complex tasks as we can track and control its exact bending configurations by measuring and controlling the joint angles, in a similar manner to robotic manipulators.

2.2. Hybrid actuator fabrication

Small differences and manual errors during fabrication can lead to significant deviations in SPAs' mechanical responses, usually resulting in an unstable and unsatisfactory repeatability in production [30]. With the introduction of rigid components, however, these issues can be well addressed as the soft component is integrated in a kinetically constrained structure. In this way, we can eliminate all the gluing and second molding process that aim to attach the stain-limiting materials onto the SPAs' body, and thus achieve the minimal manual intervention and a high efficiency in fabrication.

Therefore, a simple fabrication process is formulated for our proposed hybrid actuators. Elastosil M4601 is chosen for the molding of the soft chamber due to its good flexibility and strength upon inflation. The silicone rubber was poured into 3D-printed molds to form the soft chamber body in one step, as shown in figure 2. Then the soft chamber was dipped into the same mixer to seal one end, and a pneumatic tube was fitted to another end to form the air inlet. The rigid shells were designed in Solidworks and then 3D printed, and the whole assembly was finished by inserting the soft chamber into articulated rigid shells. Due to the existence of bump-lock structures, the relative position between the soft chamber and rigid shells can be fixed. Table 1 compares the fabrication process of typical SPAs with our hybrid actuators. Clearly, our hybrid actuators can be fabricated with minimal steps and time, featuring a high repeatability and robustness in production.

2.3. Soft-rigid interaction mechanism

We first develop an analytic model to capture the extension of the soft chamber without pneumatic pressuring and verify it using finite element method. Then we model the soft chamber bending and force exertion under the constraint of articulated rigid shells with increased input pressure.

We determine the constitutive material properties of the soft chamber using the compression and tensile test results of silicone rubber M4601 in [33]. A hyperelastic Yeoh material model is used in finite element method to capture the nonlinear characteristics of the silicone rubber with strain energy

$$U = \sum_{i=1}^{2} C_i (I_i - 3), \tag{1}$$

where I_1 and I_2 are the first and second invariant of the three principal stretches, respectively. The best-fit material coefficients are obtained as $C_1 = 0.11$ MPa and $C_2 = 0.02$ MPa. In the analytic models, we use an elastic modulus $E = 0.55$ MPa to describe the material property for simplicity also based on the compression and tensile test results.

The soft chamber can be viewed as a bellowed chamber, whose extension can be analytically modeled using elemental load cases applied to a half-convolution of a bellow [34]. When a total axial force F is applied on this half bellow, it will be separated into F_b and F_f acting on the bellow side and flat side, respectively. For the bellow side, The extension $\triangle l_b$ and the stiffness k_b are determined from

$$l_0 = nD, \tag{2}$$

$$l = \triangle l + l_0, \tag{3}$$

$$\triangle l = 4nF_b\beta, \tag{4}$$

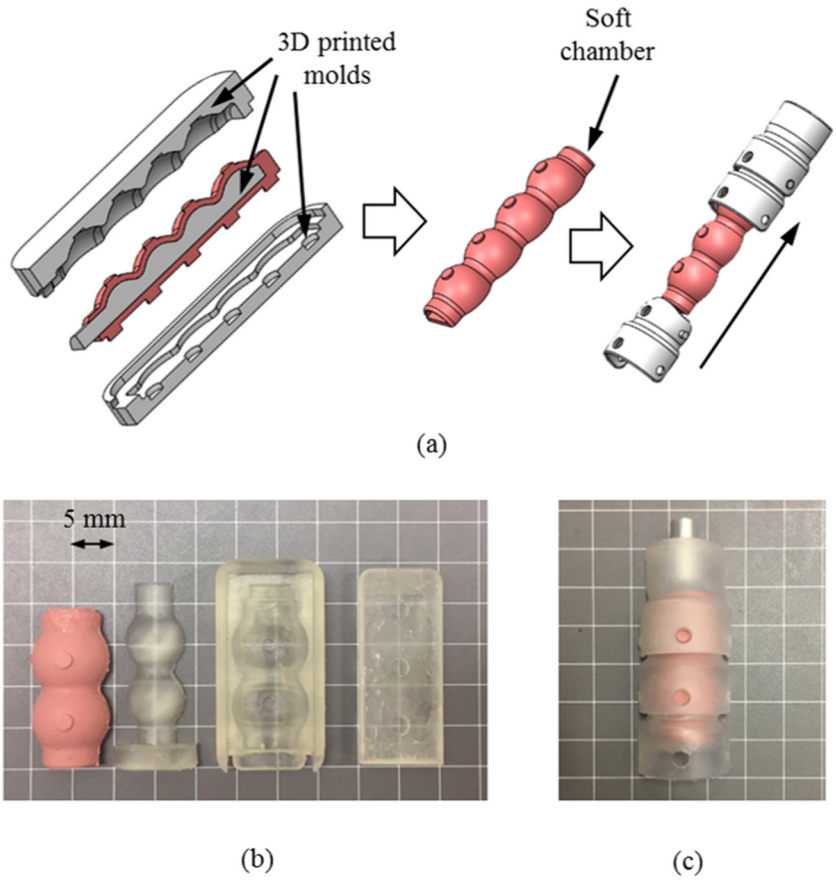

Figure 2. Fabrication process of the hybrid actuator. (a) The diagram showing the general fabrication process using one-step molding and 3D printing techniques. (b) The molds for one-step molding and the molded soft chamber. (c) The assembled hybrid actuator.

$$\beta = \frac{\pi a^3}{4EI}, \tag{5}$$

$$k_b = 1/4n\beta, \tag{6}$$

where n is the number of convolutions in the length D. l_0 is the original length of the bellow side, and l is the length after extension. β is a parameter related to the geometric parameter a, which is the average of r_1 and r_2 as shown in figure 3(a). I is the area moment of inertia of the bellow side. For the flat side, the stiffness k_f is formulated as

$$k_f = EA_b/l_0, \tag{7}$$

where A_f is the area of cross section of the flat side. The stiffness of the whole soft chamber in extension can be then obtained as $k = k_b + k_f$.

We verify this mechanical stiffness of the soft chamber by developing a 3D finite element model of a 2-convolution chamber in Abaqus. The soft chamber is pressed at one end, and the resulting displacement is compared with the prediction from the analytic model, as shown in figure 4. Clearly, a good match can be observed with a maximum error of 5% in displacement under the axial force of 1 N.

Based on the derived analytic model for the soft chamber, the geometry of the cross section can be then simplified into a semi-circle, as shown in figure 3(b). When the soft chamber is assembled into the rigid shells, the extension of the flat side will be constrained while the other side can still extend with increased pressure. This constrained extension will result in the bending of the soft chamber, and it can only bend at each joint. Therefore, the whole hybrid actuator can be viewed as a robotic manipulator with multiple degrees of freedom, as shown in figure 5. For each link, as suggested by [35], we can relate the constrained extension of the soft chamber it envelops to the joint angle θ_i as

$$\theta_i = \arctan(\triangle l'/r), \tag{8}$$

$$E_{\text{eff}} = lk_b/A_b, \tag{9}$$

$$\triangle l' = \frac{P\left[0.5\pi(r-0.5t)^2 - 2(r-0.5t)t\right]}{0.5E_{\text{eff}}\pi\left[(r+0.5)^2 - (r+0.5)^2\right]}, \tag{10}$$

where $\triangle l'$ is the extension of the equivalent semi-circular side in this link, and E_{eff} is the effective Young's modulus of the semi-circular side. This formula does not consider the energy loss caused by friction in the joints and between the soft chamber and the internal surface of the rigid shells, and therefore might overestimate the joint angle θ_i. To minimize this influence, we polished the 3D printed molds before molding and the rigid shells before the final assembling.

For a n-link hybrid actuator, its kinematics can be then described as

Table 1. Fabrication methods of typical SPAs and the hybrid actuator.

	Fiber-reinforced Actuator [6, 31]	PET shell Reinforced actuator [30]	Fabric-regulated Actuator [9]	Fiber-reinforced Actuator with fabric Patterns [32]	Hybrid Actuator [19]
Equipment	3D printer, Vacuum chamber	3D printer, Laser, Vacuum chamber	3D printer, Vacuum chamber	3D printer, Winding machine, Vacuum chamber, Cutting machine	3D printer, Vacuum chamber
Fabrication Process	Mold printing, Silicone molding, SLY[a] attaching Fiber winding, Second molding, Tip sealing	Mold printing, PET shell cutting, Silicone molding, Shell attaching, Tip sealing	Mold printing, Silicone molding, Fabric attaching, Tip sealing	Mold printing, Silicone molding, Fiber winding, Fabric attaching, Second molding, SLA[a] attaching, Tip sealing	Mold & shell printing, Silicone molding, Tip sealing, Actuator assembling

[a] Strain-limiting layer.

$$\begin{bmatrix} x \\ y \end{bmatrix} = \begin{bmatrix} \sum_{i=1}^{n} l_i \cos(\theta_1 + ... + \theta_i) \\ \sum_{i=1}^{n} l_i \sin(\theta_1 + ... + \theta_i) \end{bmatrix}. \tag{11}$$

On the other hand, the effect of the pneumatic pressure can be viewed as a torque M as suggested by [31], which can be obtained by multiplying the air pressure acting on the soft chamber tip as

$$M = \frac{2(r - 0.5t)^3 \pi P}{3\pi} - t^2 \cdot (r - 0.5t)P. \tag{12}$$

The bending stiffness of link i, which is denoted as ν_i, can be then formulated as

$$\nu_i = M/\theta_i. \tag{13}$$

If an object is placed at the hybrid actuator tip to block its further bending, an interaction force F' will be generated at the actuator tip. This force F' can be decomposed into a normal factor F_N perpendicular to the contact surface, and a frictional factor F_{fri} parallel to the contact surface. The combined interaction force F' is perpendicular to the tip link to ensure a constant bending moment arm corresponding to the tip joint, as suggested by [36]. At the tip link of an n-link hybrid actuator, the moment generated by input pressure will be separated into two parts, which will contribute to the link bending and force exertion, respectively. The relationship can be then formulated as

$$M = \nu_n \theta_n + F' l_n. \tag{14}$$

2.4. Experimental setup

To mechanically characterize the hybrid actuator and validate the proposed analytic models, we built an experimental platform that is capable to measure the actuator's bending and force capacity. As the schematic diagram shown in figure 6(a), the pneumatic pressure provided by the miniature pneumatic pump (Parker Hannifin) will be adjusted by the pressure regulator (SMC ITV2030) and then sent to the hybrid actuator. A pressure sensor (SMC ISE30) is used to measure the internal pressure of the hybrid actuator. Figure 6(b) shows overview of the testing platform. In the bending tests, one end of the hybrid actuator is firmly mounted on the testing platform, while the other end is free to bend upon inflation. Input pressure is then increased to 120 kPa in intervals of 10 kPa, and the bending motions are analyzed using the pictures taken from a camera. In the force tests, A 3-D printed rod is used to block actuator's further bending at different bending configurations, while the other end of the rod is connected to a 6-axis force/torque sensor (ATI Nano 17). The interaction force at the actuator tip can be then obtained based on the 6-axis force/torque measurement. We fabricated three hybrid actuators with degrees of freedom ranging from 1 to 3. All three hybrid actuator were characterized both in the bending and force tests. To ensure accuracy, we repeated all the tests for three times.

3. Results and discussion

3.1. Bending tests

Both bending test results obtained from experiments and model predictions are collected. Figure 7(a) presents the bending configurations of the 2-DOF hybrid actuator under 0, 50 and 100 kPa in the experiments, which are uniformly distributed along the pressure, and the trend can be clearly observed that the hybrid actuator bends downwards with increased input pressure. Moreover, in this hybrid design we can exactly define each join and link structure, and the rigid shells predefine a certain trajectory that can be more easily captured compared with that of purely soft systems. We denote the total bending angle θ_{total} as the deviation angle of the tip link, which is the summation of all joint angles, and then compare the results obtained from experimental data and model predictions as shown in figure 7(b). The analytic models are derived based on the material extension caused by pneumatic pressure, which should be zero under 0 kPa. In the experiments, however, a certain degree of pre-curling existed. To compensate this effect, the joint angle θ_i in the analytic model is then modified into

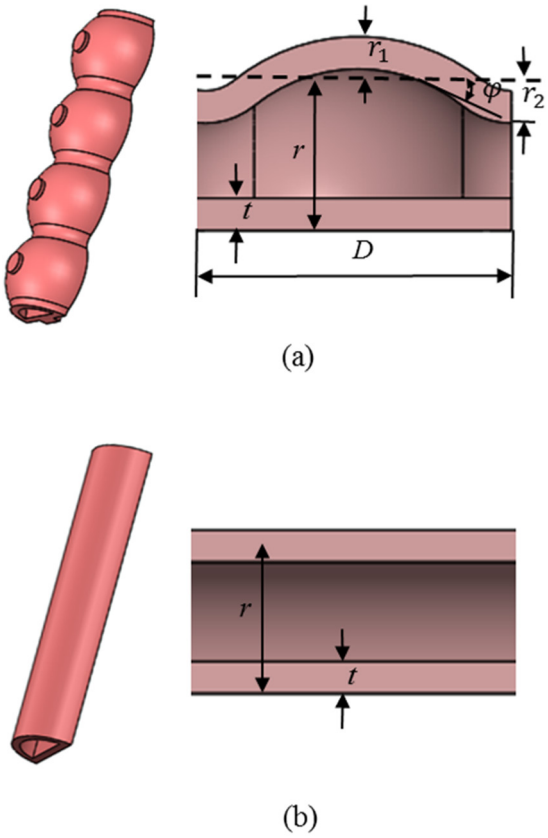

Figure 3. Geometry of the soft chamber. (a) Vertical cross-section of the soft chamber in an unflated state. (b) Vertical cross-section of the equivalent semi-circular chamber.

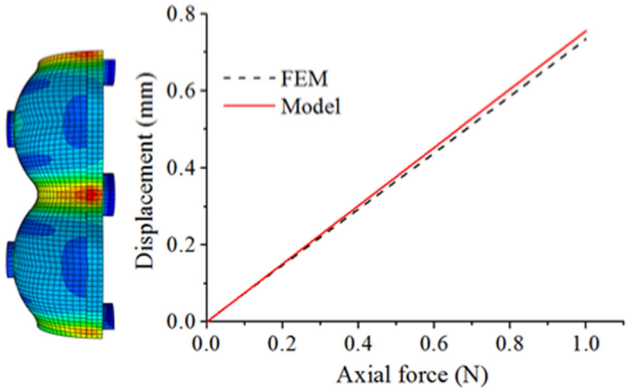

Figure 4. Comparison of the stiffness of the soft chamber obtained from finite element method and the analytic model. An axial force is applied on top of the soft chamber and resulting displacement is recorded.

$$\theta_i = \arctan(\triangle l'/r) + \theta_i', \tag{15}$$

where θ_i' is the joint angle at 0 kPa. Similar procedures are also used in other parts when analytic models are adopted. In the results presented in figure 7, a good match can be observed throughout the whole actuator bending range. The predicted results deviate from the experimental data more obviously in the 3-DOF configuration with the maximum error of 21%, and this is probably caused by the influence of gravity or friction

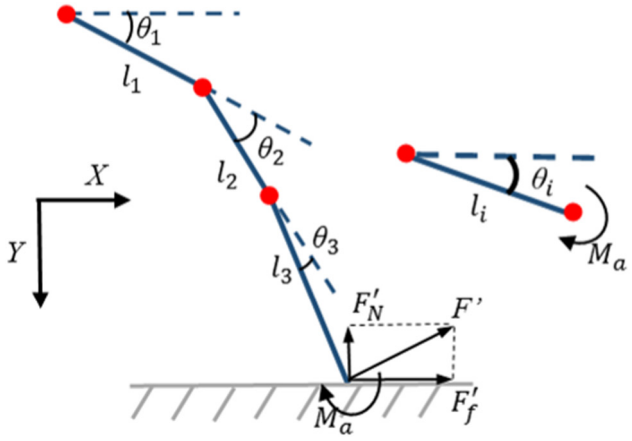

Figure 5. The equivalent robotic manipulator that the hybrid actuator can be viewed as.

that are not considered in the analytic models. Based on equation (11), the position of each joint in the bending motion can also be tracked. Figure 8 compares the bending trajectory of three configurations obtained from experiments and model predictions under 0, 50 and 100 kPa. The good match demonstrates that the models are capable of capturing the general trend of the trajectory of each joint in hybrid actuators during actuation.

To further investigate the difference in bending between hybrid actuators and purely soft actuators, we conducted a set of bending tests using only the inner soft chamber of the 3-DOF hybrid actuator. As shown in figure 9(a), the bellows of the soft chamber unfold upon actuation, and radial expansion along the whole chamber is also obvious. We compare the total bending angle of the 3-DOF hybrid actuator and the soft chamber alone in figure 9(b), and the average value of the test results are adopted for an easier comparison. In the pressure range between 0 and 50 kPa, the hybrid actuator has a similar bending capacity to the soft chamber. At higher values of pressure, however, the soft chamber incurred damage and eventually raptured due to excessive deformation.

3.2. Force tests

We also collect both the experimental and predicted data of the force tests. We conducted a series of isometric tests first, in which the 1-DOF hybrid actuator was under different bending configurations and then the force output was measured. To achieve this, four sets of tests were conducted, in which the 1-DOF hybrid actuator was first pressured to 0, 30, 60 and 90 kPa to realize four different bending configurations. The four discrete pressures were chosen uniformly in the first three quarters of the pressure range, and therefore the pressure can be further increased for the force measurement. We then used the rod connected to the force/torque sensor to block the further bending of the actuator, and the tip force can be measured through the interaction force between the actuator tip and the rod, as shown in figure 10(a). The predicted data is compared with the experimental results in figure 10(b). Both the predicted and experimental results present nearly parallel lines,

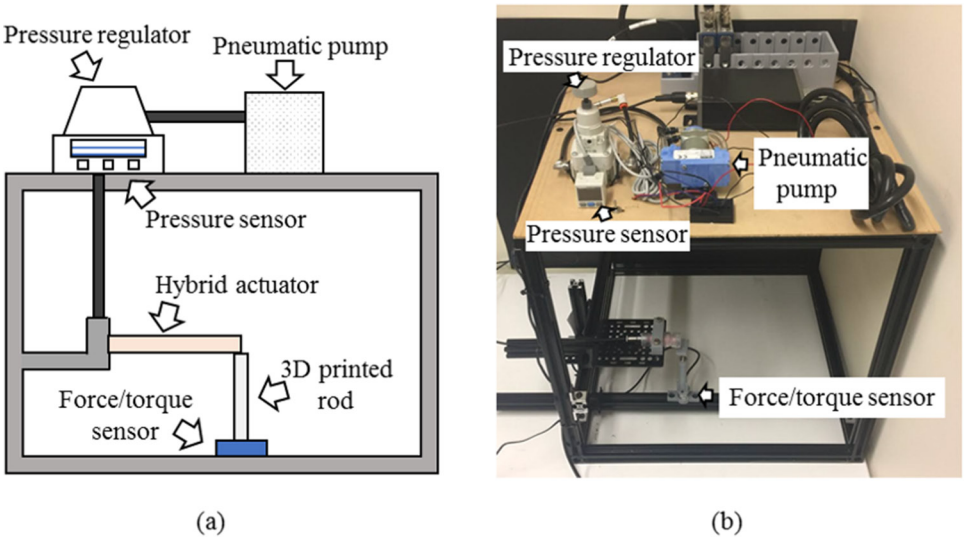

Figure 6. The testing platform. (a) The schematic diagram of the testing platform, which consists of a pneumatic pump, a pressure regulator, a pressure sensor and a force/torque sensor. (b) The overview of the testing platform.

which is consistent with the results from [36]. This is also illustrated by equation (14), as a larger part of the moment generated by input pressure will be balanced by the soft material extension at higher bending angles.

To investigate the influence of DOFs, or actuator length, on the force output, we further measured the force output of 2-DOF and 3-DOF hybrid actuators without pre-pressuring, and these results are compared with that of 1-DOF hybrid actuator in figure 11. It is noted that with higher DOFs, or actuator length, hybrid actuators tend to present reduced force exertion capacity. This trend is in conflict with the results reported by [31], in which actuator length does not have a significant influence on the force capacity of SPAs. One major cause for this difference is the different force measuring methods adopted, as we did not use a constraining platform to completely eliminate all the possible bending upon actuation. During the force tests, the hybrid actuators will keep bending with increased pressure even when interacting with an object at the tip, as shown in figure 12. In this way, the tip joint angle θ_n will keep increasing with increased pressure, which will result in an increased moment generated by material extension $\nu_n\theta_n$ and a reduced interaction force F', as suggested by equation (14). As in real application these flexible devices are not likely to be completely constrained at 0 bending angle to exert force, the force measuring method we adopt can reflect their real force exertion capacity. This phenomenon is also reported in a recent work on SPAs [37] using the similar force measuring method, and the SPAs will experience the buckling issue and deform irregularly even at relatively low pressures (less than 100 kPa). This is not likely to happen in our hybrid actuators as they are kinematically constrained in the articulated shells and can thus sustain higher pressures. Moreover, the force exertion capacity of our proposed hybrid actuators is similar to that of finger-size SPAs using the similar force measuring method [37], indicating that adopting rigid constraints does not sacrifice the force exertion capacity.

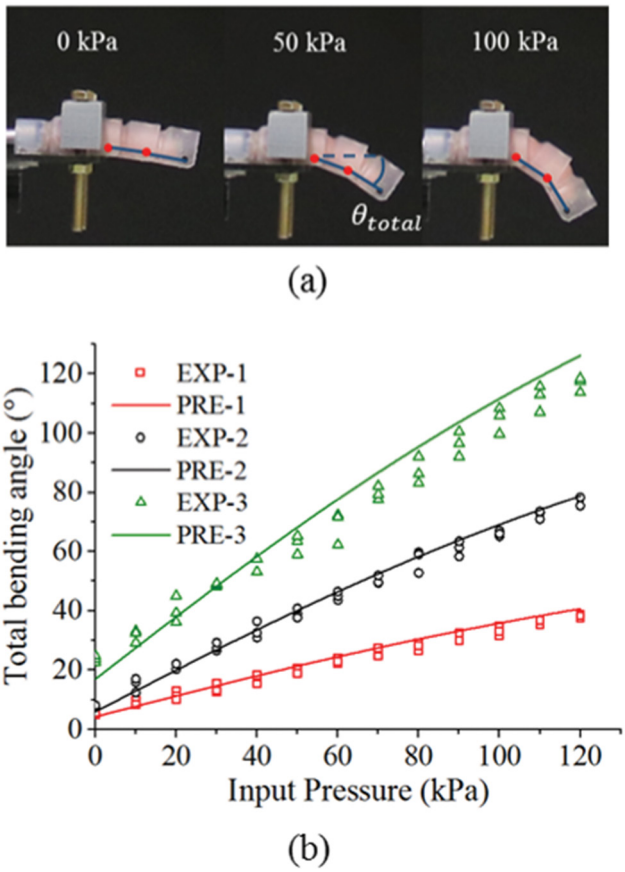

Figure 7. Bending test results. (a) The 2-DOF hybrid actuator in the bending tests under 0, 50 and 100 kPa. (b) The comparison between total bending angles obtained from experiments and model prediction of all three hybrid actuators.

The force output of the soft chamber alone is also tested. We measured the force output of the soft chamber of the 3-DOF hybrid actuator, and then compare their results as shown in figure 13. It is noted that the force output of the soft chamber is

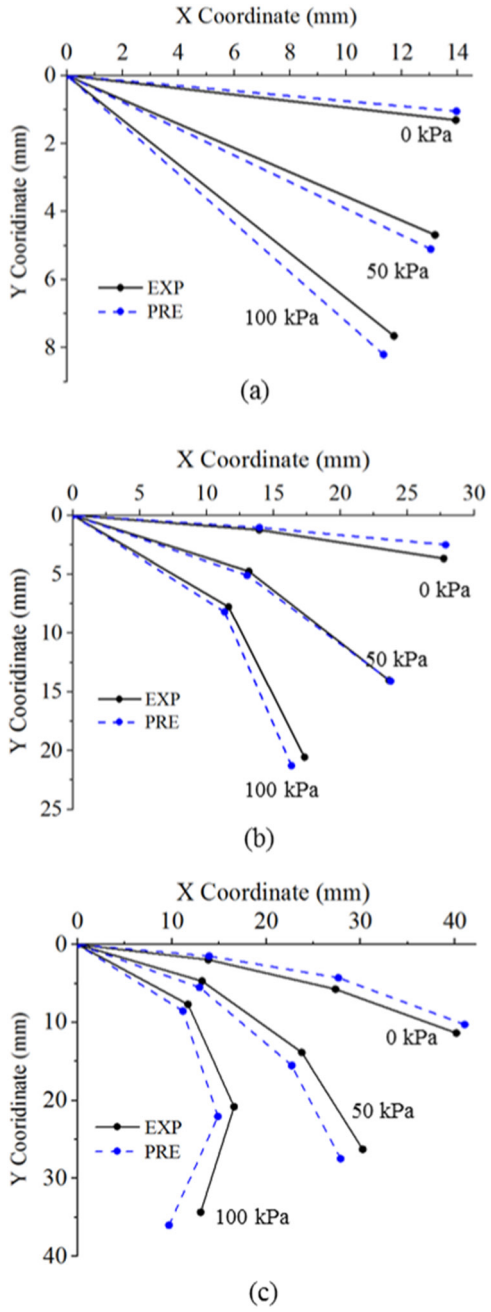

Figure 8. Comparison of bending trajectories obtained from experiments and model predictions. (a) Results of 1-DOF hybrid actuator. (b) Results of 2-DOF hybrid actuator. (c) Results of 3-DOF hybrid actuator.

significantly lower than the hybrid actuator. The radial expansion of the soft chamber is obvious upon actuation, which will generate extra stress in the soft material and lead to a lower tip force output. The soft chamber body also keeps bending with increased pressure, and this trend is more obvious than the hybrid actuator and will further decrease the force output. The input pressure was eventually increased to 50 kPa until the soft chamber raptured due to excessive stretch. For hybrid actuators, however, in all our tests no actuator failure occurred in the pressure range of 0 to 130 kPa.

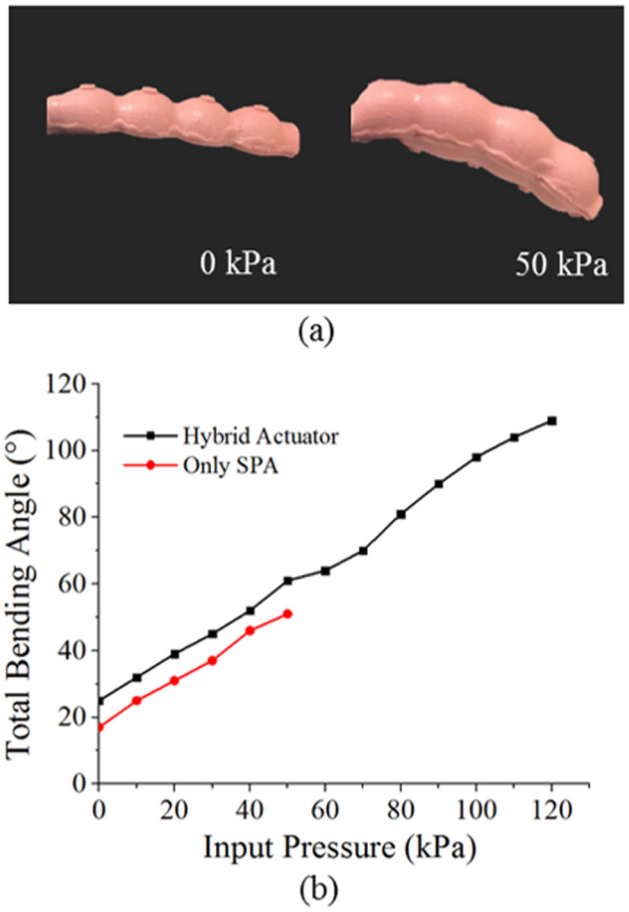

Figure 9. Comparison of the bending results obtained from the 3-DOF hybrid actuator and only the soft chamber. (a) The soft chamber in the bending tests under 0 and 50 kPa. (b) Comparison of the total bending angle of the 3-DOF hybrid actuator and the soft chamber.

3.3. Design of a robotic glove

To illustrate the potential use of our hybrid actuators, a robotic glove is assembled to assist the user in grasping daily objects. The bending configurations of hybrid actuators are similar to the bending of human fingers, and the compliant actuation provided by the soft chamber will ensure the comfortability and safety. This robotic glove adopts an open palm design, and 4 hybrid actuators with proper lengths were fabricated and then mounted on top of a glove made of neoprene. All four hybrid actuators can be independently actuated to conduct complicated tasks, while in this section they were actuated simultaneously to evaluate the feasibility of such an application. Moreover, the grasping force can be approximated using the proposed analytic models as the tip force output can be obtained with known joint angles. This provides a solution to develop control algorithms for complected tasks or optimize the design, which will be further explored in the future work.

The grasping process can be analyzed using a simplified model as shown in figure 14. The function of human fingers is not considered in this part as this glove is intended for the users with impaired finger joints. When the glove is actuated

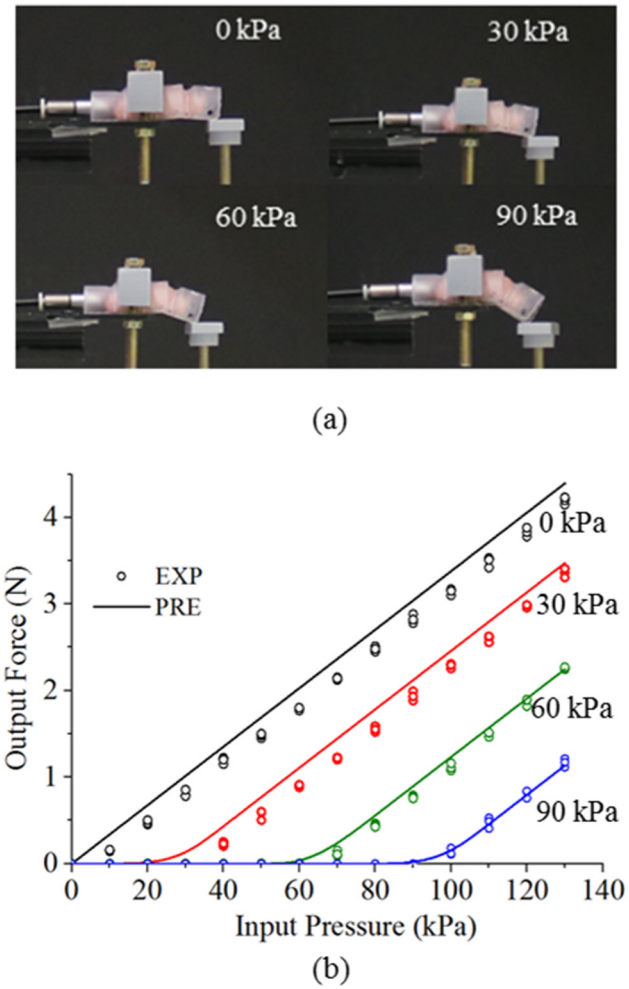

Figure 10. Force results of 1-DOF hybrid actuator at different bending configurations. (a) The 1-DOF hybrid actuator was pressured to 0, 30, 60 and 90 kPa and free to bend, and the force output was then measured. (b) The comparison of force output obtained from experiments and model predictions under pre-pressuring of 0, 30, 60 and 90 kPa.

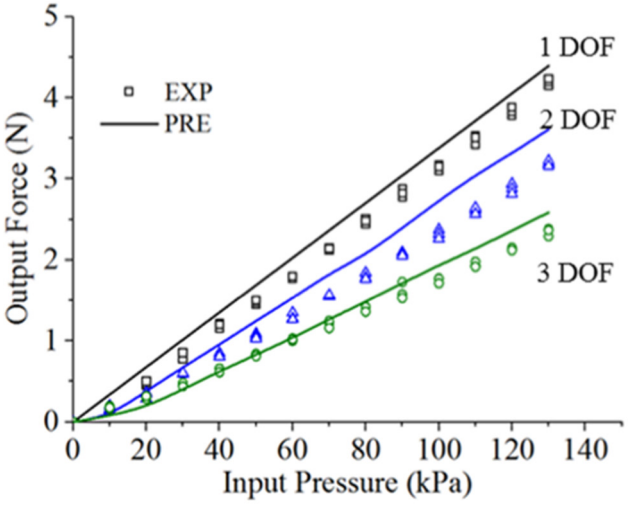

Figure 11. Comparison of force results of 1, 2 and 3-DOF hybrid actuators without pre-pressuring.

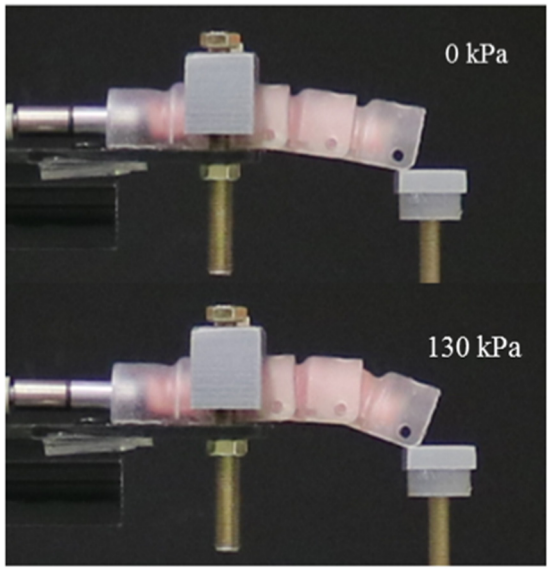

Figure 12. The increased tip joint angle of hybrid actuators in the force tests.

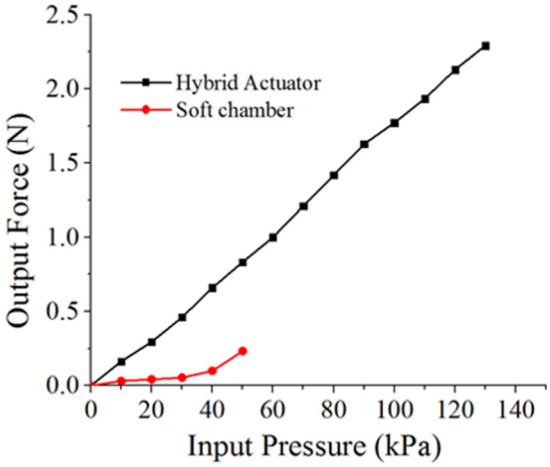

Figure 13. Comparison of the force result of the 3-DOF hybrid actuator and only the soft chamber.

with pressured air, 4 hybrid actuators will first bend to adapt to the shape of the object, and then apply an interaction force F' at the actuator tip. This interaction force F' can be divided into a horizontal force and a vertical force F, which will then balance the gravity of the object. Therefore, for a successful grasping using this robotic glove, the basic force relationship can be interpreted as

$$4F = 4F' \cos\alpha \geqslant G, \tag{16}$$

where α is the deviation angle between the interaction force F and the vertical direction.

In the tests, the user was required to wear the glove while applying no active force on their fingers. When the pneumatic pressure in four hybrid actuators was increased till 100 kPa, the hybrid actuators would assist the fingers to bend and form a closed fist, and then apply force on the objects to fulfill grasping. Different daily objects were used in the

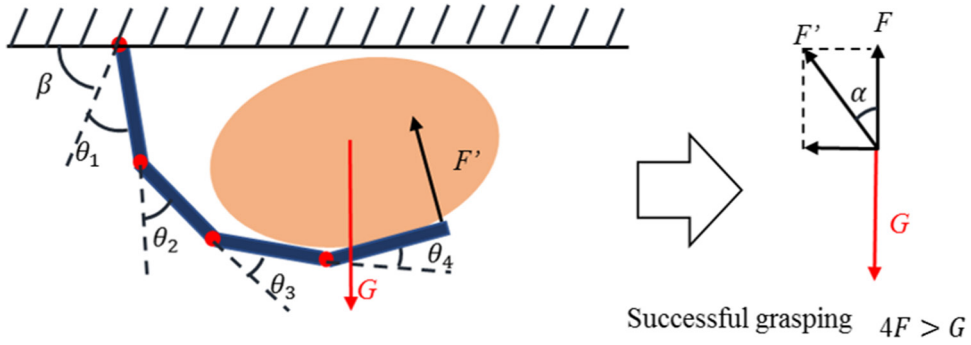

Figure 14. The simplified grasping model, in which the gravity of the object will be balanced by the vertical component of the actuator tip force.

Table 2. Grasping results obtained from analytic models.

	Gravity	Input pressure	α	F'	$4F = 4F' \cos\alpha$	Result
Eraser	0.62 N	100 kPa	66°	1.12 N	1.82 N	Successful
Solid glue	0.46 N	100 kPa	47°	0.52 N	1.41 N	Successful

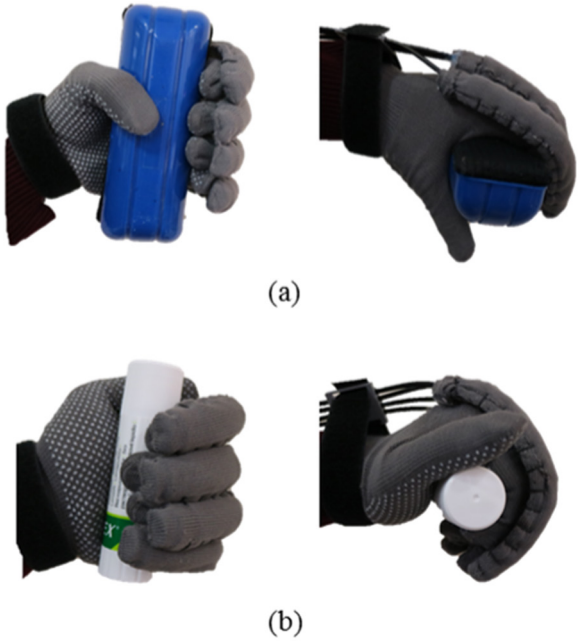

Figure 15. The grasping tasks for a user wearing the robotic glove. (a) Grasping a blackboard eraser. (b) Grasping a bottle of solid glue.

tests, including a blackboard eraser and a bottle of solid glue. Table 2 tabulates the predictions from our analytic models, and both tests satisfy equation (16) and predict successful grasping. These results are in consistent with the experimental results as shown in figure 15.

4. Conclusion

SPAs can generate desired motion and force output with a high compliance, which is ideal for applications that require safety. To date, however, generally accepted models to capture their continuous deformation are still missing, and sensing their exact bending curvature is also challenging. In this paper, we propose a hybrid actuator design with the inspiration from the abdomen of lobsters. Rigid shells are used to protect the soft chamber inside and regulate the bending into multi-link configurations, making our hybrid actuator comparable to a robotic manipulator with multiple degrees of freedom. A foolproof fabrication method is proposed that requires only basic equipment and can ensure robustness and repeatability in production. Moreover, we develop analytic models to illustrate this soft-rigid interaction mechanism, and conducted mechanical experiments to demonstrate their ability for response prediction. The actuator's kinematics can also be captured as all the joints and links can be exactly defined, which enables us to more accurately track its bending motions during actuation. Finally, a robotic glove is also to demonstrate its potentials in wearable robotic devices.

Therefore, our work indicates that the proposed hybrid actuators are readily fabricable, and can achieve both high compliance and good controllability. It is anticipated that an alternative choice besides rigid and soft robots is presented for engineering applications that require both safety and accuracy. Future work will focus on the design optimization of the hybrid actuators for an enhanced mechanical performance, and more experiments will be conducted to investigate the dynamic effects on these hybrid actuators. On the engineering side, the robotic glove will be modified to better fit the kinematics of human fingers, and a complete robotic system will be built so that users can accurately control the robotic glove to assist some daily tasks or conduct biomedical rehabilitation.

ORCID iDs

Yaohui Chen https://orcid.org/0000-0002-3308-9174
Chaoyang Song https://orcid.org/0000-0002-0166-8112

References

[1] Murray R M, Li Z and Sastry S S 1994 *A Mathematical Introduction to Robotic Manipulation* vol 29 (Boca Raton, FL: CRC Press) p 480

[2] Craig J J, Hsu P and Sastry S S 1987 *Int. J. Robot. Res.* **6** 16–28

[3] Prange G B, Jannink M J A, Groothuis-Oudshoorn C G M, Hermens H J and IJzerman M J 2006 *J. Rehabil. Res. Dev.* **43** 171

[4] Laschi C, Mazzolai B and Cianchetti M 2016 *Sci. Robot.* **1**

[5] Trivedi D, Lotfi A and Rahn C 2008 *IEEE Trans. Robot.* **24** 773–80

[6] Connolly F, Walsh C J and Bertoldi K 2016 *Proc. Natl Acad. Sci.* **114** 201615140

[7] Polygerinos P, Wang Z, Galloway K C, Wood R J and Walsh C J 2015 *Robot. Auton. Syst.* **73** 135–43

[8] Polygerinos P, Lyne S, Wang Z, Nicolini L F, Mosadegh B, Whitesides G M and Walsh C J 2013 *IEEE Int. Conf. on Intelligent Robots and Systems* pp 1512–7

[9] Yap H K, Kamaldin N, Lim J H, Nasrallah F, Goh J C and Yeow C H 2016 *IEEE Trans. Neural Syst. Rehabil. Eng.* **25** 782–93

[10] Malcolm P, Lee S, Crea S, Siviy C, Saucedo F, Galiana I, Panizzolo F A, Holt K G and Walsh C J 2017 *J. Neuroeng. Rehabil.* **14** 62

[11] Asbeck A T, De Rossi S M, Galiana I, Ding Y and Walsh C J 2014 *IEEE Robot. Autom. Mag.* **21** 22–33

[12] Zhao H, OBrien K, Li S and Shepherd R F 2016 *Sci. Robot.* **1** eaai7529

[13] White E L, Yuen M C, Case J C and Kramer R K 2017 *Adv. Mater. Technol.* **2** 1700072

[14] Paez L, Agarwal G and Paik J 2016 *Soft Robot.* **3** 109–19

[15] Onal C D, Tolley M T, Wood R J and Rus D 2015 *IEEE/ASME Trans. Mechatronics* **20** 2214–21

[16] Sun X, Felton S M, Wood R J and Kim S 2015 *IEEE Int. Conf. on Intelligent Robots and Systems* vol 2015 pp 1725–31

[17] Russo S, Ranzani T, Walsh C J and Wood R J 2017 *Adv. Mater. Technol.* **2** 1700135

[18] Chen Y, Le S, Tan Q C, Lau O, Wan F and Song C 2017 *ASME 2017 Int. Design Engineering Technical Conf. and Computers and Information in Engineering Conf. (Cleveland, Ohio, USA, 6–9 August)*

[19] Chen Y, Le S, Tan Q C, Lau O, Wan F, Song C, Sing L, Tan Q C, Lau O and Song C 2017 *IEEE Int. Conf. on Robotics and Automation (Singapore, 29 May–3 June)*

[20] Yap H K, Ng H Y and Yeow C H 2016 *Soft Robot.* **3** 144–58

[21] Ayers J 2004 *Arthropod Struct. Dev.* **33** 347–60

[22] Tshudy D, Donaldson W S, Collom C, Feldmann R M and Schweitzer C E 2009 *J. Paleontol.* **79** 961–8

[23] Factor J R 1995 *Biology of the Lobster Homarus Americanus* (Amsterdam: Elsevier) p 545

[24] Giraud-Guille M M 1998 *Curr. Opin. Solid State Mater. Sci.* **3** 221–7

[25] Boßelmann F, Romano P, Fabritius H, Raabe D and Epple M 2007 *Thermochim. Acta* **463** 65–8

[26] Sachs C, Fabritius H and Raabe D 2006 *J. Mater. Res.* **21** 1987–95

[27] Jahromi S S and Atwood H L 1976 *Can. J. Zool.* **54** 1256

[28] Newland P L, Neil D M and Chapman C J 1992 *J. Crustacean Biol.* **12** 353–432

[29] Lipcius R N and Herrnkind W F 1982 *Mar. Biol.* **68** 241–52

[30] Agarwal G, Besuchet N, Audergon B and Paik J 2016 *Sci. Rep.* **6** 34224

[31] Polygerinos P, Wang Z, Overvelde J T B, Galloway K C, Wood R J, Bertoldi K and Walsh C J 2015 *IEEE Trans. Robot.* **31** 778–89

[32] Sun Y, Yap H K, Liang X, Guo J, Qi P, Ang M H and Yeow C H 2017 *Soft Robot.* https://doi.org/soro.2016.0047

[33] Mosadegh B, Polygerinos P, Keplinger C, Wennstedt S, Shepherd R F, Gupta U, Shim J, Bertoldi K, Walsh C J and Whitesides G M 2014 *Adv. Funct. Mater.* **24** 2163–70

[34] Hermann A and Jonsson A 1997 Static characteristics of flexible bellows *MSc Thesis* University of Karlkrona/Ronneby, Sweden

[35] Drotman D, Jadhav S, Karimi M, DeZonia P and Tolley M T 2017 *IEEE Int. Conf. on Robotics and Automation* pp 5532–8

[36] Wang Z, Polygerinos P, Overvelde J, Galloway K, Bertoldi K and Walsh C 2016 *IEEE/ASME Trans. Mechatronics* **22** 717–27

[37] Sun Y, Liang X, Yap H K, Cao J, Ang M H and Yeow C H 2017 *IEEE Robot. Autom. Lett.* **2** 1